Biologically-Inspired Impedance Control with Hysteretic Damping

Nicolas Brissonneau[1], Binghan He, Gray C. Thomas, and Luis Sentis

Abstract— **Recent experiments have shown that human joints can maintain a constant damping ratio across a wide range of external loads. This behavior can be explained by the use of a "complex stiffness" frequency-domain model approximating the impedance of the human joint. However, for a robot to replicate this naturally beneficial human behavior would require a time-domain model of this nonlinear joint impedance. This paper demonstrates that there exists a nonlinear time-domain model (originally from the structural mechanics community) that has a frequency-domain "describing function" that matches the complex stiffness model observed in humans. We provide an extension of this nonlinear time-domain model that removes the need to implement hard-switching control input. In addition, we demonstrate that this proportional-and-hysteretic-damping controller has inertia-invariant overshoot and therefore offers an advantage over the more common proportional-derivative control approach. Implementing the proposed proportional-and-hysteretic-damping control in a single-joint test-robot, we demonstrate for the first time that the desired frequency domain behavior can be reproduced in practice.**

I. Introduction

While hysteretic damping was first studied by the structural and civil engineering communities, it has emerged as a model for biological joint dynamics. Structurally, hysteretic friction interfaces have been used to remove energy from vibrations in structures, with analysis performed in the frequency-domain [1], [2]. Biologically, [3] has identified the hysteretic spring model in the human elbow joint. These results were recently strengthened by [4] as they allowed for better human-adapted controller design for exoskeletons. Aside from humans, hysteretic spring behavior has also been identified in the joints of cockroaches [5]. Beyond making robots more human-like, an implementation of hysteretic damping for robot impedance control offers a frequency-independent damping ratio, which means that it could make robots more robust to overshoot due to inertia variation.

However, implementing this frequency-domain behavior in the time-domain is non-trivial, especially for researchers seeking a *linear* time-domain realization. One approach is to use a Hilbert transformation to directly convert the frequency-domain representation into a non-causal (but linear) time-domain model [6], [7]. However, since non-causal systems cannot be realized, other approaches have aimed to realize the hysteretic damping through (1) causal relaxation [8]—sacrificing the magnitude-plot behavior, (2) the addition of an all-pass filter in the frequency domain [9]—sacrificing the phase-plot behavior, and (3) a triangular-phase-plot approximation of the hysteresis loop [10]—sacrificing the linearity of the realization. According to [6], Ref. [10] "failed to realize that this is a nonlinear model," but given that robots are already nonlinear this is hardly a disqualifying drawback. As emphasized by Ref. [11], Ref. [10]'s model has "hardly received the attention it merits."

As a nonlinear approach to achieving a robustness property, an obvious comparison is adaptive control [12]. But while adaptive control aims at identifying model uncertainties and compensating for disturbances, the strength of a hysteretic damping-based controller lies in the controller's ability to provide strong robustness to inertia variation with no identification requirements.

In this paper, we investigate how to transfer human-like mass-invariant damping behavior to robots using a smoothed nonlinear realization based on [10], which we call proportional-and-hysteretic-damping (PHD) control. We show that the describing function based on position-as-input [13] for this controller exactly reproduces the desired complex-stiffness frequency response, is amplitude-invariant, and is frequency-invariant. Further novel analysis on behavior matching between PHD and PD controller designs is used to compare the two controllers in terms of their step responses and how these step responses change with inertia. We show that PHD controller has the property of being perfectly insensitive to inertia, in absolute domination of PD control's inertia-dependent overshoot. Since the model is non-linear, we also investigate the describing function based on torque-as-input to obtain a rough estimate of how consistently the desirable frequency-domain behavior will be preserved under more general conditions. And we demonstrate that the controller can be realized in hardware, with a frequency response function that closely matches both the simulations and the complex stiffness model.

II. Mathematical Preliminaries

In this section, we introduce complex stiffness and [10]'s nonlinear time-domain model—which is the basis for our PHD controller.

A. Complex Stiffness

A second-order linear mass-spring-damper can be described as a frequency domain transfer function,

$$\frac{q(s)}{\tau(s)} = \frac{1}{m \cdot s^2 + b \cdot s + k} \tag{1}$$

This work was supported by the U.S. Government, NASA Space Technology Research Fellowship NNX15AQ33H, the Office of Naval Research Grant No.N000141512507 and the National Science Foundation, Grant No.1724360. Authors are with the Department of Mechanical Engineering (N.B., B.H.), University of Texas at Austin, Austin, TX, the Department of Electrical and Computer Engineering (G.C.T.), University of Michigan, Ann Arbor, MI, and the Department of Aerospace Engineering & Engineering Mechanics (L.S.), University of Texas at Austin, Austin, TX. Send correspondence to [1] nicolasb at utexas dot edu.

with a linear damping coefficient b, a stiffness k, a mass m, a displacement q, and an input torque τ. This system has a natural frequency $\omega_0 = \sqrt{k/m}$ and a damping ratio $\zeta = b/(2\sqrt{km})$. By replacing the linear damping term bs with an imaginary component of the stiffness term hj, the *complex stiffness* model [4] is expressed as

$$\frac{q(s)}{\tau(s)} = \frac{1}{m \cdot s^2 + h \cdot j + k} \tag{2}$$

which results in a *mass-invariant* damping behavior at the resonant peaks and a hysteretic damping ratio $\zeta = h/(2k)$. However, this *complex stiffness* model is non-causal and has no exact time-domain representation.

B. A Nonlinear, Causal Approximation

To translate the human-inspired *mass-invariant* damping behavior into a time-domain system, we will need a controller for mass-like systems that behaves mostly as a spring yet which dissipates energy. Energy dissipation that does not scale with frequency can be accomplished by hysteresis, but hysteresis as typically implemented is also a highly amplitude-dependent, Coulomb-friction-like behavior that adds less and less phase lag as the input gets larger. Since complex stiffness is a linear transfer function in the frequency domain, and therefore has scale-invariant behavior, our nonlinear time-domain system should behave the same for different magnitudes of input.

This set of requirements led us both to apply a displacement-based scale factor to the Coulomb-friction hysteresis and to revisit [10]'s one-page paper that did the same in order to realize complex stiffness. The model is

$$\hat{f}_{HS} = k_{PHD} \cdot [1 + \text{sign}(q \cdot \dot{q}) \cdot \beta] \cdot q, \tag{3}$$

where $\hat{f}_{HS}$ is the resulting hysteretic spring-like force, β defines the difference between the reactive and proactive stiffness identified in Fig. 2, and k_{PHD} is their mean value shown in Fig. 1(a). This ideal model allows for instantaneous stiffness switching based on the sign of the velocity, it is more obvious when the same equation is reformulated as

$$\hat{f}_{HS} = k_{PHD} \cdot [q + |q| \cdot \text{sign}(\dot{q}) \cdot \beta]. \tag{4}$$

The switching between stiffness allows the controller to absorb the potential energy difference between the two resulting stiffnesses

$$\begin{aligned} k_1 &= k_{PHD} \cdot (1 - \beta), \text{ and} \\ k_2 &= k_{PHD} \cdot (1 + \beta). \end{aligned} \tag{5}$$

And since the switching is a function of the sign of the velocity, it results in a hysteretic damping regulated by β as shown in the comparison between Fig. 1.a and Fig. 1.d.

As shown in Fig. 2, we can now identify three phases in the dynamics of a PHD controller:

(1) proactive phase – pulls the system toward the equilibrium with low stiffness $k_1 = k_{PHD} \cdot (1 - \beta)$,
(2) transition – shows the instantaneous transition between proactive and reactive stiffness behaviors due to a velocity-sign switch,
(3) reactive phase – fights motion away from the equilibrium with high stiffness $k_2 = k_{PHD} \cdot (1 + \beta)$.

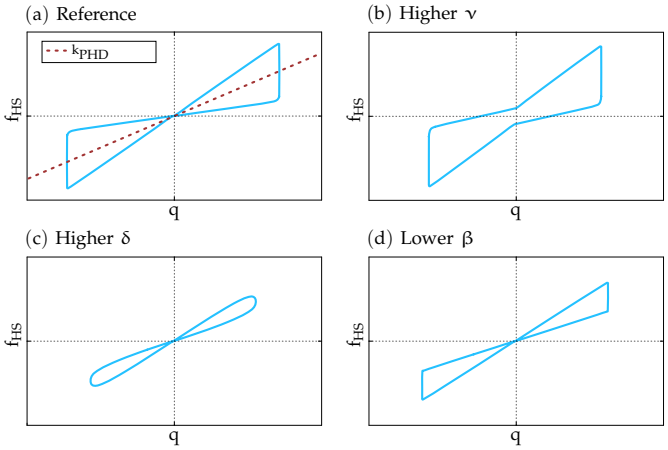

Fig. 1. **Parameters Influence**— plots of f_{HS} v.s. q show the influence of different ν, δ, and β values in (b), (c), and (d) compared to a reference parameter setting in (a) over a full period. ν and δ are defined in Sec .IV-A.

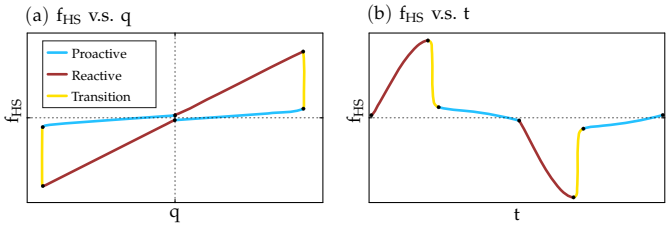

Fig. 2. **PHD controller force period**— (a) shows the 3 phases describing the dynamics of the PHD controller in the force to position plane, while (b) shows the associated time response of f_{HS}.

One can notice that the transitions remain short and thus the dynamics of the controller are dominated by the reactive and proactive stiffness phases.

III. Model Analysis

In this section, we provide a thorough analysis of the mass-invariant behavior of (4).

A. Percentage Overshoot

Because our controller is composed of two stiffnesses, k_1 and k_2, we can predict the step response overshoot (Fig. 3). This is because this response is switching between two second-order linear behaviors when the velocity changes sign.

We can analytically calculate the amount of overshoot using conservation of energy. The potential energy equality $\frac{1}{2} \cdot k_1 \cdot {q_1}^2 = \frac{1}{2} \cdot k_2 \cdot {q_2}^2$ holds between subsequent peaks in amplitude, q_1 and q_2. And therefore,

$$\frac{|q_2|}{|q_1|} = \sqrt{\frac{k_1}{k_2}}. \tag{6}$$

Substituting (5), the percentage overshoot ϕ_{PHD} of controlling a mass m using the proposed PHD controller can be expressed as

$$\phi_{PHD} = 100 \cdot \frac{|q_2|}{|q_1|} = 100 \cdot \sqrt{\frac{1 - \beta}{1 + \beta}}. \tag{7}$$

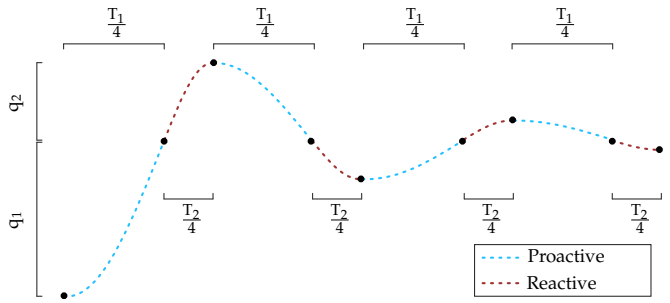

Fig. 3. **Illustration of Step Response Behavior**—This figure illustrates the contribution of each stiffness due to a step input in the time-domain.

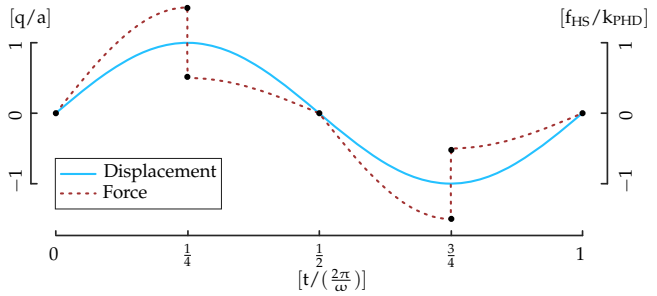

Fig. 4. **Conceptual Plot of Sinusoidal Response**— a representation of each stiffness contribution to a sinusoidal response in the time domain.

B. Damped Natural Frequency

Considering again the step response behavior in Fig. 3, the response of a PHD controller is defined by the consecutive switch between two stiffness k_1 and k_2. The switching happens when q or $\dot{q}$ crosses zero. We can split the full period into four quadrants, such that each quadrant is the result of a single linear spring behavior:

$$T_{PHD} = 2 \cdot \frac{T_1}{4} + 2 \cdot \frac{T_2}{4}, \tag{8}$$

where T_1 and T_2 are the duration of the full periods of the mass-spring dynamics solely dominated by k_1 and k_2. Let us define ω_1 and ω_2 as the natural frequencies of the mass m with virtual springs k_1 and k_2. By substituting $T_1 = \frac{2\pi}{\omega_1}$, $T_2 = \frac{2\pi}{\omega_2}$, and $T_{PHD} = \frac{2\pi}{\omega^d_{PHD}}$ into (8), we can express the damped natural frequency ω^d_{PHD} as

$$\omega^d_{PHD} = \frac{2 \cdot \omega_1 \cdot \omega_2}{\omega_1 + \omega_2}, \tag{9}$$

Substituting $\omega_1 = \sqrt{k_1/m}$ and $\omega_2 = \sqrt{k_2/m}$ into (9), we obtain

$$\omega^d_{PHD} = \frac{2 \cdot \sqrt{k_1 \cdot k_2}}{\sqrt{k_1 \cdot m} + \sqrt{k_2 \cdot m}}. \tag{10}$$

Substituting k_1 and k_2 from (5) we get

$$\omega^d_{PHD} = \sqrt{\frac{k_{PHD}}{m} \cdot \frac{2 \cdot (1-\beta^2)}{1 + \sqrt{1-\beta^2}}}. \tag{11}$$

C. Time-Domain Comparison between PD and PHD

The percentage overshoot, ϕ_{PD}, of a PD controller and its damped natural frequency, ω^d_{PD}, for a linear impedance controller described in (1) can be expressed as

$$\begin{aligned} \phi_{PD} &= 100 \cdot e^{-\frac{\zeta \cdot \pi}{\sqrt{1-\zeta^2}}}, \\ \omega^d_{PD} &= \sqrt{\frac{k_{PD}}{m} \cdot (1-\zeta^2)}. \end{aligned} \tag{12}$$

If we let $\phi_{PD} = \phi_{PHD}$, (7) can be written as

$$\beta = \frac{1 - e^{-2 \cdot \frac{\zeta \cdot \pi}{\sqrt{1-\zeta^2}}}}{1 + e^{-2 \cdot \frac{\zeta \cdot \pi}{\sqrt{1-\zeta^2}}}}. \tag{13}$$

where $\zeta = b_{PD}/(2 \cdot \sqrt{k_{PD} \cdot m})$. If we also let $\omega^d_{PD} = \omega^d_{PHD}$, we can calculate the value of k_{PHD} as

$$k_{PHD} = k_{PD} \cdot (1-\zeta^2) \cdot \frac{1 + \sqrt{1-\beta^2}}{2 \cdot (1-\beta^2)}. \tag{14}$$

Based on (13) and (14), k_{PHD} and β can be expressed in terms of m, k_{PD} and b_{PD}. For any PD control parameter setting, there exists a pair of k_{PHD} and β such that the time response of the mass m with the PHD controller matches the time response of m with the PD controller.

D. Frequency-Domain Response

When position is the input and force is the output, we can analytically derive the describing function [13] of the control in (4). In contrast to previous analytical solutions for torque-forced oscillations [14], this will yield a describing function that exactly reproduces the complex stiffness. Let $q(t) = a\cos(\omega t)$, such that it represents the phasor $1 + 0j$. Within a single $2\pi/\omega$ period (as shown in Fig. 4), the output $f(t)$ will be

$$f_{HS}(t) = \begin{cases} k_2 \cdot a \cdot \cos(\omega t), & \text{for} \quad 0 \le t \le \frac{\pi}{2\omega}, \\ k_1 \cdot a \cdot \cos(\omega t), & \text{for} \quad \frac{\pi}{2\omega} \le t \le \frac{\pi}{\omega}, \\ k_2 \cdot a \cdot \cos(\omega t), & \text{for} \quad \frac{\pi}{\omega} \le t \le \frac{3\pi}{2\omega}, \\ k_1 \cdot a \cdot \cos(\omega t), & \text{for} \quad \frac{3\pi}{2\omega} \le t \le \frac{2\pi}{\omega}. \end{cases} \tag{15}$$

Since a appears linearly in all four cases, the describing function will have no dependence on amplitude and we will assume without loss of generality that $a = 1$.[1] We can calculate the describing function, $\hat{f}(\omega)$, through the Single Period Phasor Transform of [15],

$$\hat{f}_{HS}(\omega) = \frac{\omega}{\pi} \int_0^{2\pi/\omega} f(t) \cdot e^{-j\omega t} dt, \tag{16}$$

or by re-parameterizing in terms of $\theta = \omega t$ as in [13],

$$\hat{f}_{HS}(\omega) = \frac{1}{\pi} \int_0^{2\pi} f(\theta/\omega) \cdot e^{-j\theta} d\theta. \tag{17}$$

Using this second form, we can break the integral into simple trigonometric integrals,

$$\begin{aligned} \hat{f}_{HS}(\omega) = \frac{1}{\pi} \Bigg[& k_2 \int_0^{\frac{\pi}{2}} \cos^2(\theta) + j \cdot \cos(\theta)\sin(\theta) d\theta \\ & + k_1 \int_{\frac{\pi}{2}}^{\pi} \cos^2(\theta) + j \cdot \cos(\theta)\sin(\theta) d\theta \end{aligned}$$

[1] We omit phase-shift due to an equally obvious invariance property.

$$+ k_2 \int_{\pi}^{\frac{3\pi}{2}} \cos^2(\theta) + j \cdot \cos(\theta)\sin(\theta) d\theta$$
$$+ k_1 \int_{\frac{3\pi}{2}}^{2\pi} \cos^2(\theta) + j \cdot \cos(\theta)\sin(\theta) d\theta \Big], \quad (18)$$

which can be simplified by exploiting the indefinite integrals $\int \cos^2(\theta) d\theta = \theta/2 + \sin(\theta)\cos(\theta)/2$ and $\int \cos(\theta)\sin(\theta) d\theta = -\cos^2(\theta)/2$,

$$\hat{f}_{HS}(\omega) = \frac{2k_2}{\pi}\left(\frac{\pi}{4} + \frac{1}{2}\cdot j\right) + \frac{2k_1}{\pi}\left(\frac{\pi}{4} - \frac{1}{2}\cdot j\right), \quad (19)$$

or more simply

$$\hat{f}_{HS}(\omega) = k_{PHD}\left(1 + \frac{2\beta}{\pi}\cdot j\right). \quad (20)$$

While describing function analysis is designed to handle very general classes of nonlinear systems, this system is scale-, phase-, and even frequency- invariant. More importantly, it meets our goal by taking the form of a complex stiffness.

IV. Methods

A. Tuning Parameters

The controller shown in (4) assumes perfect knowledge of the sign of velocity and displacement, but these are corrupted by noise in reality. To add extra energy dissipation for small oscillations and smooth the torque transitions where velocity changing sign, we add extra parameters ν and δ such that (4) becomes

$$f_{HS} = k_{PHD}\cdot q + \frac{(k_{PHD}\cdot\beta\cdot|q| + \nu)\cdot\dot{q}}{|\dot{q}| + \delta}, \quad (21)$$

where

(1) δ softens the transition phases (Fig. 2) and acts as a dead zone for velocities (Fig. 1.c), and
(2) ν provides a minimum energy dissipation when q gets close to 0 (Fig. 1.b).

B. Simulation Strategy

To prove the effectiveness of the proposed PHD controller in (21), we conduct simulations of a 1-DOF system defined as

$$\ddot{q} = \frac{1}{J}\cdot(\tau_g + \tau_{FF} + \tau_{FB}), \quad (22)$$

where τ_g is the gravity torque, τ_{FF} is a feed-forward term for gravity compensation, and τ_{FB} is a feedback term for tracking a reference state $[q_{des},\ \dot{q}_{des}]$. Using our PHD controller,

$$\tau_{FB} = k_{PHD}\cdot\Delta q + \frac{(k_{PHD}\cdot\beta\cdot|\Delta q| + \nu)\cdot\Delta\dot{q}}{|\Delta\dot{q}| + \delta}, \quad (23)$$

where $\Delta q = q_{des} - q$ and $\Delta\dot{q} = \dot{q}_{des} - \dot{q}$. On the other hand, for a PD controller, τ_{FB} is implemented as

$$\tau_{FB} = k_{PD}\cdot\Delta q + b\cdot\Delta\dot{q}. \quad (24)$$

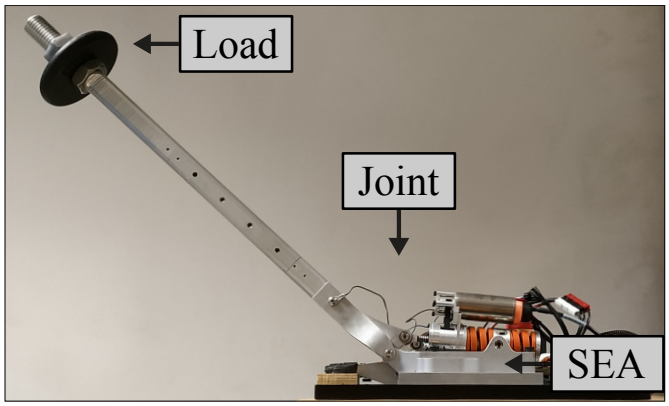

Fig. 5. **Test Apparatus**—a modified Taurus Testing System with a P-170 Orion actuator (Apptronik Systems Inc., Austin, TX).

TABLE I
Controller Parameters

Index	k_{PHD}	β	δ	ν
T.1	38.64	0.57	0.003	0.001
T.2	81.81	0.88	0.003	0.001
T.3	323.08	0.98	0.003	0.001
F.1	52.79	0.76	0.314	0.100

C. Time-Domain Step Response Tests

We generate step responses using the proposed PHD and PD controllers to compare their robustness to inertia variations. For each pair of PHD and PD controllers, we test three inertia values: 15, 50, and 300 $\mathrm{kg}\cdot\mathrm{m}^2$, with 50 serving as the nominal value. To provide a practical comparison between controllers, we match the amount of overshoot and the damped natural frequency for a nominal inertia using (13) and (14).

Tab. I shows the parameters for three PHD controllers (T.1-3). T.1 is compared to a PD controller with $k_{PD} = 30\ \mathrm{N}\cdot\mathrm{m}$ and $b_{PD} = 15.5\ \mathrm{N}\cdot\mathrm{m}\cdot\mathrm{s}$. T.2 is compared to a PD controller with $k_{PD} = 30\ \mathrm{N}\cdot\mathrm{m}$ and $b_{PD} = 31.0\ \mathrm{N}\cdot\mathrm{m}\cdot\mathrm{s}$. And T.3 is compared to a PD controller with $k_{PD} = 30\ \mathrm{N}\cdot\mathrm{m}$ and $b_{PD} = 46.5\ \mathrm{N}\cdot\mathrm{m}\cdot\mathrm{s}$. The nominal damping ratios for these three PD controllers are 0.2, 0.4, and 0.6.

We chose values for δ and ν such that they remain as minimal as possible to preserve the desired property of the controller while being high enough to mitigate chattering. Due to the near-ideal simulation environment, we are able to easily remove chattering by using very low values for δ and ν.

D. Frequency-Domain Response Tests

Our time domain model is motivated by the frequency domain complex stiffness model. Here, we are interested in comparing the complex stiffness model (2) with the frequency-domain behavior achieved by (21).

In order to plot the ideal complex stiffness model, we need only add an inertia term to (20):

$$\frac{\tau(s)}{q(s)} = m\cdot s^2 + k_{PHD}\cdot\frac{2\beta}{\pi}\cdot j + k_{PHD}. \quad (25)$$

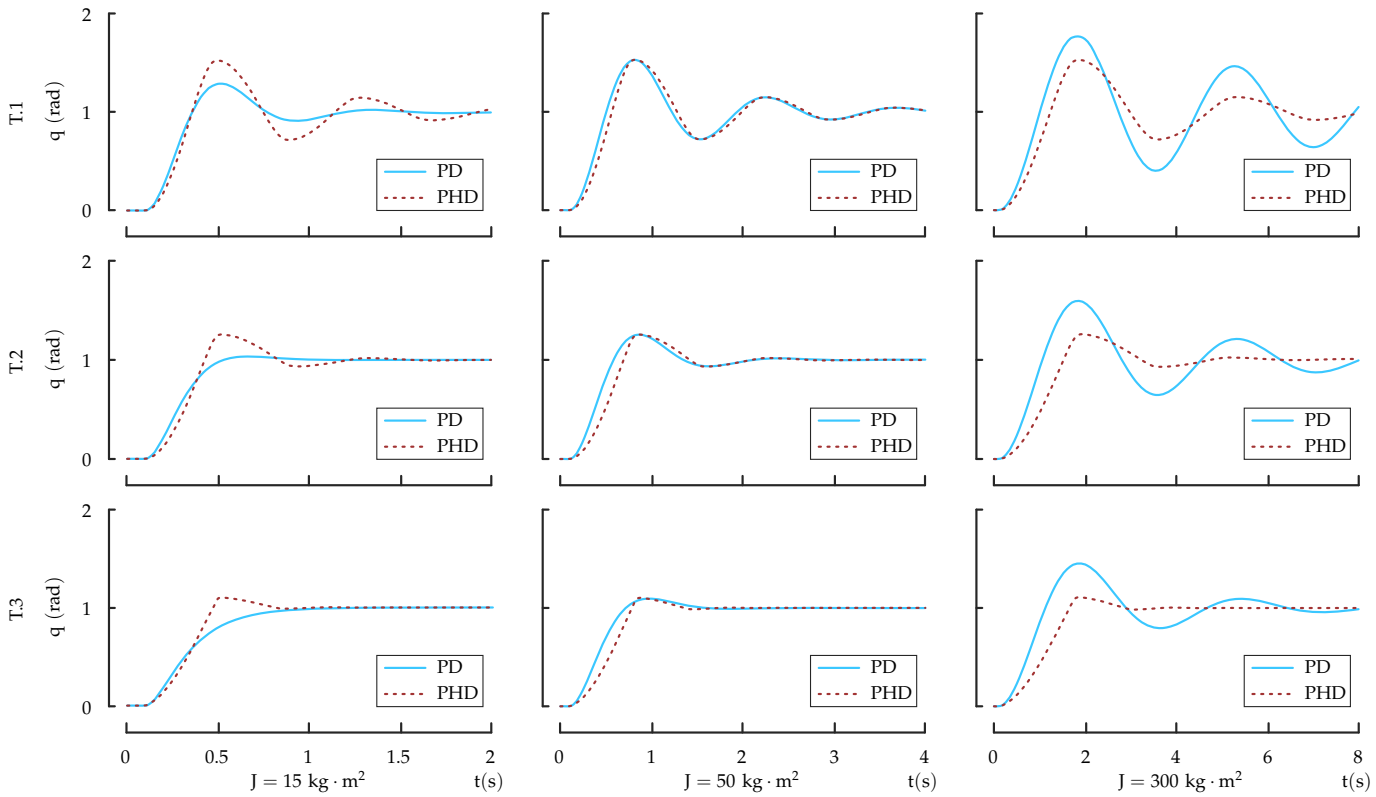

Fig. 6. **Step-response comparison between PD and PHD controllers**—The middle-column corresponds to the damped natural frequencies and overshoots being matched between PD and PHD controllers, while the left and the right columns respectively correspond to a decrease and an increase of the system's inertia. These plots demonstrate the robustness from the PHD controller to inertia variations by showing a near constant overshoot regardless of the load.

One way for measuring the frequency-domain response of the PHD controller is to perform frequency-domain system identification using a sinusoidal input for $q_{des}(t)$ and measuring the torque output $\tau(t)$ while using the PHD controller F.1 defined in Tab. I. The reason why F.1 has different parameters than T.1 through T.3 is because we found its values feasible in the real hardware.

Because the hardware will not be following an ideal sinusoidal position input for identification, we also simulate a more hardware-realistic case where the closed-loop system's natural dynamics are forced by a torque disturbance. For this type of experiment, (22) becomes

$$\ddot{q} = \frac{1}{J} \cdot (\tau_g + \tau_{FF} + \tau_{FB} + \tilde{\tau}), \tag{26}$$

where $\tilde{\tau}$ is a chirp perturbation of torque input.

To confirm our simulations we perform experiments in the hardware testbed shown in Fig. 5 [16]. δ is set to match the noise level in the velocity signal—to avoid noise-driven output chattering. ν is set to be well under the input amplitude, which is sufficient for eliminating startup transients in finite time. To de-noise the velocity signal $\dot{q}$, we employ a second order low-pass filter with $\omega_c = 120$ rad/s.

The parameters of the PHD controller (F.1) for the frequency-domain test are shown in the last row of Tab. I. For each frequency-domain test, the PHD controller moves the arm of the testbed which has a moment of inertia of 0.187 $\text{kg} \cdot \text{m}^2$. The input chirp signal has amplitude 4 $\text{N} \cdot \text{m}$ and sweeps frequencies within $[4, 40]$ rad/s.

V. Results

A. Comparison Between PD and PHD

The first set of results are shown in Fig. 6. The middle column shows the step responses with the nominal inertia, $J = 50\ \text{kg} \cdot \text{m}^2$, where the PD and PHD controllers are chosen to have the same values for the damped natural frequency and amount of overshoot. Therefore the response from the two controllers is almost identical. The response using the PD controller become more damped with $J = 15\ \text{kg} \cdot \text{m}^2$ and overshoot more with $J = 300\ \text{kg} \cdot \text{m}^2$ than using the PHD controller. On the other hand, the step responses using the PHD controller change very little with the changes of the moment of inertia. Therefore, the PHD controller demonstrates a superior robustness to inertia variations as anticipated.

B. Frequency-Domain Results

Fig. 7 shows the Bode plots of the complex stiffness model described in (25) and the three frequency-domain system identification results using (21): 1) a simulated system identification plot using q_{des} as the input, 2) a simulated system identification plot using $\tilde{\tau}$ as the input, and 3) a hardware experiment using $\tilde{\tau}$ as the input. As expected, the describing function measured with position as an input and the complex stiffness model are similar to each other. In addition the

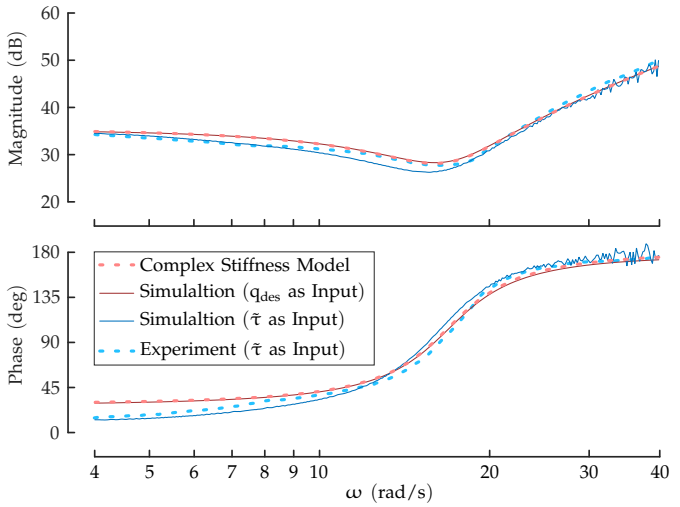

Fig. 7. **Frequency domain behaviors comparison**— This figure shows the behavior of the proposed complex stiffness model and three frequency-domain system identification results using (21): 1) a simulated system identification plot using q_{des} as the input, 2) a simulated system identification plot using $\tilde{\tau}$ as the input, and 3) a hardware experiment using $\tilde{\tau}$ as the input.

describing functions measured with force as input are also similar to each other. Between 8 and 20 rad/s the experiment seems to adhere closer to the position as input than the torque as input describing functions. This is likely due to the effect of the low-level actuator controller [16] which limits the torque control bandwith. Naturally, the two types of inputs converge at high frequencies because the mass of the system dominates and causes both position and torque to approach sinusoidal behavior.

Between the two simulations, the magnitude and phase plots have distinct features including a smaller low frequency phase asymptote and a smaller magnitude before the resonant frequency for the torque-as-input models. This low frequency behavior is explained mainly by the torque-as-input behavior spending a longer time in the proactive than in the reactive phase. In addition, as we increase δ, we further reduce the phase at lower frequencies.

VI. Discussion

Mass-invariant overshoot promises to be a practical robustness property that achievable by mechanical and robotic systems. In this paper we have demonstrated that 1) PHD control offers superior inertia robustness compared to classic PD controllers, 2) PHD control has comparable behavior to the complex stiffness model in the frequency domain, and 3) a hardware realization of PHD control can successfully achieve this complex stiffness behavior. This hardware implementation relied on implementing a time-domain approximation of hysteretic damping with extra parameters ν and δ to remove chattering and provide extra energy dissipation.

Robots that manipulate partially known objects, or more generally, robots that need strong guarantees for overshoot regardless of the loads they carry, stand to benefit from this approach. The mass-invariance property avoids complicated tuning or system identification.

Because our PHD controller switches between stiffnesses, it is slightly more sensitive to delays than a classic PD controller; and this is a key factor in tuning the controller. While one might be tempted to tune for low overshoot, tuning a PHD controller means compromising between speed and energy dissipation. It can be shown, that the energy absorbed by the controller is a function of the ratio between k_1 and k_2 which is ultimately defined by β. So one might think that it is desired to have a very high k_2 value. But if there is a delay in the transition from low stiffness to high stiffness, the system can gain energy at the transition. This puts a practical upper limit on how large k_2 can become before the time delay will add more energy than the system can remove.

References

[1] M. Wang, T. Zan, Y. Yang, and R. Fei, "Design and implementation of nonlinear tmd for chatter suppression: An application in turning processes," *International Journal of Machine Tools and Manufacture*, vol. 50, no. 5, pp. 474–479, 2010.

[2] L. Tong, Y. Zhang, X. Zhou, A. Keivan, and R. Li, "Experimental and analytical investigation of d-type self-centering steel eccentrically braced frames with replaceable hysteretic damping devices," *Journal of Structural Engineering*, vol. 145, no. 1, p. 04018229, 2018.

[3] E. J. Perreault, R. F. Kirsch, and P. E. Crago, "Multijoint dynamics and postural stability of the human arm," *Experimental brain research*, vol. 157, no. 4, pp. 507–517, 2004.

[4] B. He, H. Huang, G. C. Thomas, and L. Sentis, "Complex stiffness model of physical human-robot interaction: Implications for control of performance augmentation exoskeletons," in *2019 IEEE/RSJ International Conference on Intelligent Robots and Systems (IROS)*. IEEE, 2019, pp. 6748–6755.

[5] D. M. Dudek and R. J. Full, "Passive mechanical properties of legs from running insects," *Journal of Experimental Biology*, vol. 209, no. 8, pp. 1502–1515, 2006.

[6] J. A. Inaudi and J. M. Kelly, "Linear hysteretic damping and the hilbert transform," *Journal of Engineering Mechanics*, vol. 121, no. 5, pp. 626–632, 1995.

[7] J. A. Inaudi and N. Makris, "Time-domain analysis of linear hysteretic damping," *Earthquake engineering & structural dynamics*, vol. 25, no. 6, pp. 529–545, 1996.

[8] N. Makris, "Causal hysteretic element," *Journal of engineering mechanics*, vol. 123, no. 11, pp. 1209–1214, 1997.

[9] A. Keivan, B. M. Phillips, M. Ikenaga, and K. Ikago, "Causal realization of rate-independent linear damping for the protection of low-frequency structures," *Journal of Engineering Mechanics*, vol. 143, no. 9, p. 04017058, 2017.

[10] T. J. Reid, "Free vibration and hysteretic damping," *The Journal of the Royal Aeronautical Society*, vol. 60, no. 544, p. 283–283, 1956.

[11] A. Bountis, K. Kaloudis, and C. Spitas, "Periodically forced nonlinear oscillators with hysteretic damping," *Journal of Computational and Nonlinear Dynamics*, 2020.

[12] P. A. Ioannou and J. Sun, *Robust adaptive control*. Courier Corporation, 2012.

[13] A. Gelb and W. E. Vander Velde, *Multiple-input describing functions and nonlinear system design*. McGraw-Hill Book Company, 1968.

[14] T. Caughey and A. Vijayaraghavan, "Free and forced oscillations of a dynamic system with "linear hysteretic damping"(non-linear theory)," *International Journal of Non-Linear Mechanics*, vol. 5, no. 3, pp. 533–555, 1970.

[15] G. C. Thomas and L. Sentis, "Mimo identification of frequency-domain unreliability in seas," in *American Control Conference (ACC)*. IEEE, 2017, pp. 4436–4441.

[16] N. Paine, S. Oh, and L. Sentis, "Design and control considerations for high-performance series elastic actuators," *IEEE/ASME Transactions on Mechatronics*, vol. 19, no. 3, pp. 1080–1091, 2014.